# Method and Analysis of Spectrally Compressed Radio Images for Mobile-Centric Indoor Localization

J. Talvitie, Member, IEEE, M. Renfors, Fellow, IEEE, M. Valkama, Senior Member, IEEE, E. S. Lohan, Senior Member, IEEE

**Abstract**—Large databases with Received Signal Strength (RSS) measurements are essential for various use cases in mobile wireless communications and navigation, including radio resource management algorithms and network-based localization. Because of the constantly increasing number of radio transmitters with various wireless technologies and with the advent of 5G cloud computing and Internet of Things (IoT), the required size of the RSS databases are becoming unmanageably large. Thus, the requirements for the bandwidth and data rates for accessing the memory might become too costly. Therefore, in order to reduce the size of the RSS database, while maintaining the data quality, we have previously proposed a method of spectrally compressed RSS images, which is able to achieve considerable data compression of up to 70%. In this paper, we present a comprehensive analysis of the spectral compression process and identify the main error sources, which affect the compression performance. Based on the analysis, we propose a novel theoretical framework and methods to optimize the performance of the spectral compression. In addition, we derive the Cramér-Rao Lower Bound (CRLB) for the RSS-based localization error and compare the CRLB between separate baseline localization approaches. The theoretical analysis is justified and compared with experimental RSS measurements taken from several multi-storey buildings.

**Index Terms**—Data compression, Indoor positioning, Wireless Local Area Networks, Received Signal Strength, Fingerprinting

## 1 INTRODUCTION

MEMORY is a scarce resource and currently, it is estimated that the average amount of memory required by mobile applications grows at a rate higher than 50% per year [1]. Mobile localization is rapidly becoming a standard requirement not only as an enabler of Location-Based Services (LBS), but also for location-based optimization of wireless network operation. Mobile-centric localization solutions are especially demanding in terms of memory consumption and low-cost data compression solutions are highly important in this context.

Due to wide availability of Received Signal Strength (RSS) measurements in communications networks, RSS-based localization has become as one of the most studied network-based localization approaches [2]-[7]. The vast majority of the RSS-based localization systems are learning-based, meaning that the user location estimate is based on pre-collected learning data from the target area. In this case, the RSS measurements from the observed radio transmitters (TX) together with the measurement coordinates are stored beforehand in the learning database. By the TX notation we refer to any transmitting radio device in a fixed location from which the RSS measurement can be obtained, such as Wireless Local Area Network (WLAN) access points, Bluetooth devices and cellular network base stations. After this, in the localization phase, the RSS measurements of the user are compared with the learning database in order to estimate the user location.

Since both the requirements for the localization accuracy and the number of available TXs (along with the number of accessible mobile networks) have been increasing, the size of the learning database has become a considerable challenge. Because of this, in addition to the obvious growth of the required memory space, there is also the need to increase the capacity of the data traffic to/from the database. Thus, in order to reduce the database complexity, radio propagation Path Loss (PL) models have been proposed, for example, in [9]-[11]. With PL models the database size can be significantly reduced compared to the traditional fingerprinting approach studied, for example, in [12]-[14]. However, with the PL models, the smaller database size is achieved at the cost of reduced database quality and localization accuracy. In addition to the PL models, also other database compression methods have been studied in the literature. One approach, which is also considered as a benchmark in this paper, is to use clustering methods studied, for example, in [15]-[16]. In this approach, the database size reduction is achieved via classification of RSS measurements, where the measured RSS levels together with measurement location coordinates are considered as separable features of the database. Other compression approaches include compressive sensing and sparse representations of the RSS measurements studied, for example, in [17]-[19], as well as matrix completion methods studied in [20]. Besides reducing the database size, the methods in [17]-[20] can be used to reduce the effort of exhaustive learning data collection, which is out of the

• *J. Talvitie, M. Renfors, M. Valkama and E.S. Lohan are with the Laboratory of Electronics and Communications Engineering, Tampere University of Technology, P.O.Box 692, FI-33101 Tampere, Finland. E-mails: jukka.talvitie@tut.fi, markku.renfors@tut.fi, mikko.e.valkama@tut.fi, elena-simona.lohan@tut.fi.*

main focus of this paper. By difference with [15]-[20], the developed algorithms presented in this paper aim at global-scale indoor localization systems, where the learning data can be obtained by using crowdsourcing-based methods. By global scale we refer to algorithms working at a country level or even at continent level, not only in a certain building or groups of buildings. Although the introduced algorithms are developed to meet the needs of a global-scale localization system, several important design features, such as crowdsourcing methods and database management protocols, are not within the scope of this paper.

In [21] we have introduced a novel approach using spectrally compressed radio images to reduce the size of the learning database, while maintaining the localization accuracy at the level of traditional fingerprinting. The main idea in the proposed approach has been to utilize the Discrete Cosine Transform (DCT) to reveal the spectral content of the radio images. Due to spatial correlation of RSS measurements, the energy of the frequency domain presentation is concentrated on a few DCT coefficients, which are then stored in the database. Besides the DCT, also other frequency transforms, such as Discrete Fourier Transform (DFT) are applicable for the spectral compression. However, since the DCT has been widely applied in numerous data compression applications, especially regarding image and audio processing, it was chosen to be used also in this paper. Moreover, whereas the DFT introduces a complex-valued frequency spectrum, the DCT spectrum is purely real-valued. Therefore, since RSS measurements are given in real-valued numbers, with DCT it is possible to completely avoid handling of complex numbers in the data processing and analytical derivations.

Despite of the fact that the proposed approach is fundamentally a lossy compression method, the localization accuracy can be even improved compared to the traditional fingerprinting approach, as shown in [21]. This can be explained by the noise filtering property of the compression approach, as shown later with the analytical results in this paper. In addition, due to the noise filtering, the proposed compression method can also improve the tolerance of device heterogeneity and detection of measurement outliers. These would enable calibration-free localization methods and reduced database maintenance costs. Moreover, the main applications of the proposed spectral compression method are in RSS-based wireless localization and mobile-centric RSS studies, but such model can find its applicability also in RSS-based radio resource management, adaptive handovers and network planning.

As the initial idea of the proposed spectral compression was introduced in [21], in this paper we focus on introducing a new analytical framework to analyze and justify the proposed WLAN fingerprinting compression method. Moreover, by introducing appropriate physical models, we conduct a deep and comprehensive analysis of the used compression algorithms. Thus, the main contributions of this paper are:

- Describing and discussing physical radio propagation models to justify the efficiency of the proposed spectral compression approach
- Analyzing the proposed spectral compression approach by deriving the energy of compression error, noise error and total error for the spectrally compressed RSS data. In addition, we introduce the variance of a location likelihood function for the considered localization approaches and show that it is possible to achieve the smallest variance with the proposed spectral compression approach
- Introducing a method for the optimal selection of DCT coefficients to enhance the database quality
- Deriving a Cramér-Rao Lower bound (CRLB) of the location estimator and studying the effects of different system parameters on the achievable localization accuracy via the CRLB
- Providing indoor localization results from multiple buildings with experimental RSS measurements and comparing them with the newly-derived CRLB

The remaining part of the paper is organized as follows. In Section 2 we derive the fundamental model for the RSS measurements. In addition, we present our experimental RSS measurement set and explain the structure of the RSS-based learning database. In Section 3 we describe the considered localization approaches, including the definition of location likelihood function and the description of requirements for the learning database size. After this, in Section 4, we focus on the selection of the DCT coefficients and analyze separate error sources found in the spectral compression. Finally, in Section 4 we study the CRLB between separate localization approaches, which we then use in the comparison with the experimental RSS measurement results in Section 6.

## 2 Measurement Model and Learning Database

### 2.1 Experimental Measurement Set

We have collected experimental RSS data from five separate multi-storey buildings in Finland and Germany, including two shopping malls, one office building, and two office-like university buildings, whose characteristics are further shown in Table 1. All measurements are based on the beacon signals of WLAN 802.11 [22] access points at the 2.4 GHz carrier frequency. The measurement device was a Nexus 7 tablet by ASUSTeK Computer Inc. (ASUS, Android 4.3.1 OS), which included proprietary measurement software with proprietary indoor maps. In addition, regarding the experimental results shown in Section 6, we have also collected measurements from the 4-storey university building with 2 additional devices, including Huawei 360 U61 mobile phone and Huawei T1 7.0 tablet. These measurements are merely used to compare the performance of the proposed spectral compression approach with other considered localization approaches in the case of having multiple devices for collecting the learning data and user tracks.

The coordinates of the RSS measurement locations were determined manually by using building floor maps. At each location, the RSS measurements from the heard access points were stored into the database. As described later in Section 2.3, in order reduce the overall database size, the RSS measurements are mapped into a fixed 5 m x 5 m grid.

TABLE I
BUILDINGS CHARACTERISTICS FOR THE EXPERIMENTAL RSS DATA (5 X 5 M GRID STEP)

| Building location | Building type | Approx. area of a floor [m²] | No. of floors | No. of heard TXs | No. of grid points |
|---|---|---|---|---|---|
| Finland | Univ. | 6000 | 4 | 422 | 559 |
| Finland | Univ. | 10000 | 3 | 402 | 182 |
| Finland | Office | 3500 | 6 | 1103 | 354 |
| Finland | Mall | 16000 | 3 | 424 | 768 |
| Germany | Mall | 20000 | 6 | 468 | 1633 |

In case that multiple RSS measurements from the same access point are heard in the same location, the stored RSS value is defined as the arithmetic mean over the RSS measurements. Depending on the building, there are often several (even up to hundreds) of RSS measurements obtained by a single access point at one grid point location.

During the collection of experimental measurements, we have tried to introduce a scenario similar to crowdsourcing-based data collection, where the device orientation and radio propagation environment, such as human mobility, cannot be controlled. Furthermore, in order to study the localization accuracy, the measurement campaign was separately organized for the learning data collection and for the user test track collection. Part of the collected measurement data is publicly available [23].

### 2.2 Measurement Model

RSS measurements are affected by the radio propagation distance and the radio propagation environment including shadowing. The correspondence between the RSS measurement and the distance between the measurement location and the TX location can be described with the PL models as studied, for example, in [10]-[11] and [24]. On top of this, obstacles and alteration in the radio propagation environment generate shadowing and other types of RSS fluctuation around the PL-model-based RSS values.

In learning-data-based localization systems, it is important that observed RSS values in separate locations remain as immutable as possible with respect to time. In case of stationary obstacles, such as large furniture and walls, the shadowing effect is considered to be unique and time-invariant for each location. However, the variations in the orientation of the measurement device and in the heading of the measurer together with any other changes in the radio environment, cause time-variant shadowing. This is unique for each separate RSS measurement, even if the measurements would be taken at the same location.

Radio wave propagation characteristics in multi-floor buildings are generally asymmetric in vertical and horizontal directions. This is because floor losses are typically considered to be much higher compared to corresponding wall losses. Therefore, in our studies, we assume a floor-wise RSS measurement model in order to reduce the complexity of asymmetric 3D models. However, in case of multi-floor scenarios, the presented model can be utilized in the context of spectrally compressed RSS images for each floor separately, as done later in this paper.

Now, by considering a single RSS measurement from a single TX in an arbitrary location $(x,y)$, the model of RSS measurement (in dBm) can be written as

$$P(x,y) = Q(x,y) + S(x,y) + W\,, \tag{1}$$

where $Q(x,y)$ and $S(x,y)$ define the PL-model-based RSS and the stationary shadowing value at the location coordinate $(x,y)$, and $W$ is a time-variant shadowing term, respectively. Here, the stationary (time-invariant) shadowing term $S(x,y)$ introduces RSS fluctuations due to stationary obstacles in the radio path, including walls and fixed furniture. The time-variant shadowing term $W$ describes the RSS fluctuation due to moving obstacles, such as human mobility, body losses and opening/closing doors.

As the values of $Q(x,y)$ and $S(x,y)$ are fixed at the considered location, all the variations in the RSS levels (e.g., due the movement of the measurement device or other objects in the radio path) are induced by $W$. From the localization point of view, the PL model $Q(x,y)$ along with the stationary shadowing term $S(x,y)$ are the essential part of the RSS measurement model, since in a fixed location their values do not fluctuate between the learning data phase and the localization phase. On the contrary, as the term $W$ introduces temporal variations, it can be seen as an undesired noise term. In addition, if different types of devices are used to collect the data, the resulting RSS level fluctuation between the devices can be incorporated in $W$.

We assume that the PL model $Q(x,y)$ follows the simple log-distance model [24] as

$$Q(x,y) = A - 10n\log_{10}(d(x,y))\,, \tag{2}$$

where $A$ and $n$ are the PL constant (i.e. RSS at 1m distance) and the PL exponent, and $d(x,y)$ is the distance between the measurement location $(x,y)$ and the TX location $(x_{TX},y_{TX})$ as

$$d(x,y) = \sqrt{(x-x_{TX})^2 + (y-y_{TX})^2}\,. \tag{3}$$

Although we have considered our modeling only in 2D, it is possible to extend it to cover also the 3D case by simply adding the vertical coordinate in the above propagation distance definition. However, when using 3D models in multi-storey buildings, one should pay attention to floor losses, which can significantly impact on the accuracy of the PL models. For this reason, we use only 2D models, but in case of multi-storey buildings, 2D models can be used in a floor-wise manner as done in [21]. Moreover, we have not restricted the characterization of the PL model in anyway, but other PL models can also be utilized by simply replacing $Q(x,y)$ with the desired PL model definition.

Changing the PL model and its parameters affects the average observed RSS values in the system. Moreover, it is well known that high-level RSS measurement contribute more on the localization accuracy compared to low-level RSS measurements. Furthermore, a similar effect on the average RSS levels can be obtained also by changing the average distances between the TXs in the network. Some studies on the effect of PL model parameters on the localization accuracy have been conducted in [25]. Nonetheless, it should be noticed that using the proposed approach of spectrally compressed RSS images does not require any prior information on the PL models, but the PL

models are required in the analytical derivations, as they form an essential part of radio propagation characteristics. Thus, in practice the PL models are fundamentally invisible and intrinsic to the proposed spectral compression methods, as the stored spectral components comprise information on the spatially correlated RSS observations regardless of the underlying propagation mechanisms.

Since $S(x,y)$ is a result of stationary obstacles in the radio path, nearby RSS measurements are correlated. Moreover, since neither building floorplans or furniture layouts are expected to be known, the shadowing term $S(x,y)$ is considered to be a Gaussian distributed random variable as $S \sim N(0, \sigma_S^2)$, where $\sigma_S^2$ is the shadowing variance. To model the spatial correlation we choose to use the conventional Gudmundson model given in [26]. Hence, the covariance between two locations, $(x_1,y_1)$ and $(x_2,y_2)$, can be modelled as

$$Cov\left(S(x_1,y_1), S(x_2,y_2)\right) = \sigma_S^2 e^{\left(-\frac{\Delta d}{D_{corr}}\right)}, \quad (4)$$

where $\Delta d$ is is the Euclidian distance between the coordinates $(x_1,y_1)$ and $(x_2,y_2)$, similar to (3), and $D_{corr}$ is a decorrelation distance parameter, which affects the magnitude of the correlation. Again, we do not restrict the correlation model to the above-mentioned, but any other model can also be used in the analysis.

For simplicity, we assume that the time-variant shadowing term $W$ (i.e. the noise term causing the RSS fluctuation in a fixed location) is a Gaussian distributed random variable as $W \sim N(0, \sigma_W^2)$. In practice, the distribution itself including its properties, such as skewness or kurtosis, varies depending on the measurement location and the radio environment as studied in [27]-[28]. However, since there is no clear resolution to which distribution has the best fit, we justify our selection of the Gaussian distribution based on the central limit theorem.

### 2.3 The Structure of the Learning Database

During the learning data collection phase, the RSS measurements from the heard TXs are stored with the measurement coordinates, obtained either manually or automatically. Moreover, to reduce the number of stored measurements in the database, the measurements are often mapped into a synthetic grid with predefined measurement coordinates. The magnitude of the grid interval should be defined based on the localization requirements and on the magnitude of spatial correlation of the RSS measurements. In addition, by using the grid multiple measurements can be obtained for the same location, which can be used to reduce the effect of measurement outliers in the database.

After the learning data collection, there are in total $N_{FP}$ fingerprints including RSS measurements from one or several TXs as

$$\left\{x_i, y_i, \left\{\Omega_{RSS,i,r} : r \in \Omega_{TX}\right\} : i = 0,\ldots, N_{FP}-1\right\}, \quad (5)$$

where $x_i$ and $y_i$ are the grid mapped x-coordinate and y-coordinate of the $i^{th}$ fingerprint, $\Omega_{RSS,i,r}$ is the set of all RSS measurements taken from the $r^{th}$ TX in the $i^{th}$ fingerprint, $\Omega_{TX} = \{0,1,\ldots N_{TX}-1\}$ is the set of all TX indices used to identify the TXs, and $N_{TX}$ is the total number of TXs in the database. In case of multiple-floor scenario, the database structure can be easily extended by including an additional floor coordinate besides $x_i$ and $y_i$. Now, if multiple measurements from the same TX are heard in the same fingerprint (i.e., there are more than one measurement in $\Omega_{RSS,i,r}$), the stored RSS value is determined as the arithmetic mean over the RSS measurements. Thus, the learning database can be further described as

$$\left\{x_i, y_i, \left\{P_{i,r} : r \in \Omega_{TX}\right\} : i = 0,\ldots, N_{FP}-1\right\}, \quad (6)$$

where $P_{i,r}$ is the arithmetic mean of the RSS measurements found in $\Omega_{RSS,i,r}$.

By considering the RSS measurement model in (1), the useful information for the localization is found from $Q(x,y)$ and $S(x,y)$, as their values are fixed for a given location. Thus, by taking the average of several RSS measurements from the same location, it is possible to reduce the variance of the noise term $W$ as

$$W_{i,r} = N\left(0, \frac{\sigma_W^2}{N_{MEAS,i,r}}\right), \quad (7)$$

where $W_{i,r}$ and $N_{MEAS,i,r}$ are the noise term and the number of averaged RSS measurements for the $i^{th}$ fingerprint and $r^{th}$ TX. This reduced variance is a result of a Maximum Likelihood (ML) based sample mean estimator obtained by taking the mean of the RSS measurements [29]. Nonetheless, here we assume that separate RSS measurements are independent, which practically means that there should be enough diversity in the measurement campaign. In other words, RSS measurements from the same location should be taken in different times and with different device orientations.

In Fig. 1, we have presented the fundamental process to construct the databases for fingerprinting, PL-modeling and spectrally compressed RSS images. In addition, we have illustrated the required database sizes in percent with respect to the traditional fingerprinting approach as well as the relative Signal-to-Noise Ratio (SNR) of the databases from the localization point-of-view. Thus, by SNR we refer to the ratio between the location-dependent part of the stored RSS data (e.g. $Q(x,y)$ and $S(x,y)$ in (1)) and the noise power (e.g. $W$ in (1)), as discussed later in Section 4.

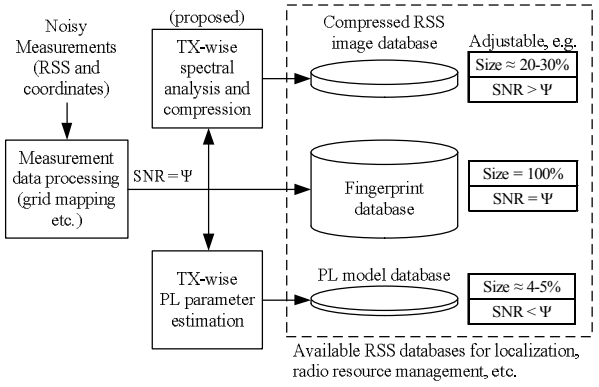


Fig. 1. An illustration of the considered RSS databases. The database sizes have been given with respect to the conventional fingerprint database according to the results shown in Section 6. The SNR refers to the quality of the RSS measurements/data with respect to the localization application.

## 3 DESCRIPTION OF THE LOCALIZATION APPROACHES

In order to enable a fair comparison between the considered localization approaches (i.e., fingerprinting, PL-modeling and spectrally compressed RSS images) we use the same ML principle with each one them. Furthermore, we will show that the only difference between the approaches is in the variance of the likelihood function, which explains the performance difference between the proposed spectral compression approach and the other approaches shown earlier in [21]. Thus, in this Section, we first define the likelihood function and the considered ML-based location estimates, which are common to all the considered localization approaches. Then, we study the variance of the likelihood function separately for each approach, and finally, determine the required size of the corresponding learning databases.

### 3.1 Likelihood Function and Location Estimate

To estimate the user location we have chosen the probabilistic Bayesian approach used earlier, for example, in [30]. With the Bayesian approach, we rely on the assumption on the correctness of the RSS measurement model, from which the required location likelihood function is derived. Furthermore, by assuming independent RSS measurements from separate TXs, the likelihood function at the fingerprint location $\mathbf{x}_i=[x_i, y_i]^T$ can be given as

$$p(\Omega_{RSS,USER} \mid \mathbf{x}_i) = \prod_{r \in \Omega_{TXheard}} p_{RSS,i,r}\left(P_{USER,r} - P_{i,r}\right), \quad (8)$$

where $\Omega_{RSS,USER} = \left\{P_{USER,r} : r \in \Omega_{TXheard}\right\}$ is the set of all heard user RSS measurements, $P_{USER,r}$ is the user RSS measurement from the $r^{\text{th}}$ TX, and $\Omega_{TXheard} \subset \Omega_{TX}$ is the set of the heard TX indices, and $p_{RSS,r,i}(\cdot)$ is the probability density function of the RSS measurement at the $i^{\text{th}}$ fingerprint of the $r^{\text{th}}$ TX. Now, based on the measurement model, given in (1), the RSS variations in each location are completely defined by the time-variant shadowing term $W$, and thus, $p_{RSS,r,i}(\cdot)$ is a Gaussian distribution. Different to the learning data RSS values, in which multiple measurements can be used to reduce the variance of the time-variant shadowing term, there is always only one RSS measurement per TX available for the user. Nevertheless, by introducing appropriate Bayesian tracking algorithms, such as in [10], multiple measurements from a fixed location would eventually filter out the noise. However, this is considered to be out of the scope of this paper.

Based on the Bayes' rule, and assuming that no a priori information on user location is available, the posterior probability density function of the user location $\mathbf{x}_{USER}$ is directly proportional to the likelihood function and can be given as

$$p(\mathbf{x}_{USER} \mid \Omega_{RSS,USER}) \propto \sum_{i=0}^{N_{FP}-1} p(\Omega_{RSS,USER} \mid \mathbf{x}_i)\chi_i(\mathbf{x}_{USER}), \quad (9)$$

where

$$\chi_i(\mathbf{x}_{USER}) = \begin{cases} 1, & \text{if } \mathbf{x}_{USER} \text{ is mapped to the } i^{\text{th}} \text{ fingerprint} \\ 0, & \text{otherwise} \end{cases} \quad (10)$$

is an indicator function, which applies the posterior function over the whole coordinate space (i.e., not just at the fingerprint coordinates). Hence, based on the above, the Maximum A Posteriori (MAP) estimate of the user location can be obtained by choosing the maximum of the posterior function. However, based on our studies better performance can be obtained by taking a weighted mean of the posterior function as

$$\hat{\mathbf{x}}_{USER} = \sum_{i=0}^{N_{FP}-1} \frac{p\left(\Omega_{RSS,USER} \mid \mathbf{x}_i\right)}{\sum_{j=0}^{N_{FP}-1} p\left(\Omega_{RSS,USER} \mid \mathbf{x}_j\right)} \mathbf{x}_i, \quad (11)$$

which can be further considered as a MMSE-based location estimate. Here, it is worth mentioning that in consequence of the weighted sum in (11), in which the weights are determined by the likelihood functions, the location estimates are not restricted to the actual fingerprint grid points. This enables the use of relatively sparse grids without significantly losing estimation resolution.

### 3.2 Definition of the variance of the likelihood function

#### 3.2.1 Fingerprinting

In conventional fingerprinting, the learning data is used in the localization without any additional data processing or compression. Therefore, by considering the RSS measurement model in (1), and taking into account the reduced noise variance due to the RSS averaging in the learning phase, given in (7), the overall variance of $p_{RSS,r,i}(\cdot)$ is given as

$$\sigma^2_{FP,i,r} = \sigma^2_W \left(\frac{1}{N_{MEAS,i,r}} + 1\right), \quad (12)$$

where we have reasonably assumed that the time-variant fading term $W$ of the user RSS measurement and the averaged learning data noise term $W_{i,r}$ are not correlated. Therefore, the total variance is simply a sum of the variances of $W_{i,r}$ and $W$.

#### 3.2.2 PL-model-based approach

In PL-model-based approach, the learning database RSS values are first used to estimate PL model parameters for each TX, such as $A$ and $n$ shown in (2). For this model the least squares estimate of the PL parameters can be obtained as shown in [10]. However, since the PL model is a function of a distance to the TX, it is also required to estimate the TX locations. This can be done, for example, either by using the weighted centroid approach shown in [28] and [31], or a joint parameter estimation approach studied in [10].

Instead of using the traditional trilateration-based localization principle, as done in [32]-[33], we exploit the idea of recreated fingerprints as in [34], where the RSS values are regenerated in the target area based on the stored PL parameters. This enables us to use the same likelihood principle as with the other localization approaches.

In the fingerprinting approach the learning data RSS values carry location based information from both the PL model term $Q(x,y)$ and the stationary shadowing term $S(x,y)$. However, the PL modeling approach can only capture the

information related to the PL model $Q(x,y)$. Therefore, from the PL-model-based localization point of view, $S(x,y)$ can be seen as an additional noise term, whose power is directly given by the shadowing variance $\sigma_S^2$. Now, assuming ideal PL parameter estimates, the overall variance of the probability density function $p_{RSS,r,i}(\cdot)$ in the likelihood function can be defined as

$$\sigma_{PL,i,r}^2 = \sigma_W^2 \left( \frac{1}{N_{MEAS,i,r}} + 1 \right) + \sigma_S^2 . \quad (13)$$

Of course, in practice there would be some additional variance on top of this due to the errors in the PL parameter estimation. However, here $\sigma_{PL,i,r}^2$ can be considered to be the lower bound of the observed variance in the PL modeling approach.

### 3.2.3 Spectrally compressed RSS images

In the spectral compression of RSS images, it is required to take a DCT transformation of the database RSS values per TX. In most of the cases, in order to enable this, appropriate interpolation and extrapolation, for example, by using methods studied in [34], are required to complete the grid of the RSS values for each TX. Although interpolation and extrapolation have an essential role in the spectral compression approach, a detailed optimization of them is considered to be out of the scope of this paper. However, since interpolation and extrapolation introduce new RSS values for new locations in the learning data, the used methods have to be carefully selected. As discussed in [34], one safe approach is to use linear interpolation techniques, but also other techniques are feasible, such as Gaussian regression methods which use the knowledge of spatial correlation in estimating the RSS levels. Besides interpolation and extrapolation techniques, it is also possible to define the frequency transform via non-uniform DCT (or DFT), where uniform grid values are not required. However, due to increased complexity, we have left the research on non-uniform transformations for future studies.

After appropriate interpolation and extrapolation of RSS values, for each TX we have a uniform rectangular grid (i.e. the RSS image), which is presented by the matrix $\mathbf{G}$ as in [21]. For the sake of simplicity of the notations, we have extracted the TX index $r$ from the RSS image analysis, since the analysis is always done in TX-wise manner. Moreover, handling RSS images from different TXs at a same time is only necessary in the localization phase. Due to the fact that the DC component of $\mathbf{G}$ (i.e., the mean RSS value) is typically considerably larger compared to the other spectral components, the mean of the image is removed as

$$\mathbf{G}_0 = \mathbf{G} - \mu, \text{ where } \mu = \frac{1}{MN} \sum_{i=0}^{M-1} \sum_{j=0}^{N-1} [\mathbf{G}]_{ij} , \quad (14)$$

where $\mathbf{G}_0$ is the zero mean RSS image, $[\mathbf{G}]_{ij}$ is the $i^{\text{th}}$ row and $j^{\text{th}}$ column element of the matrix $\mathbf{G}$, $\mu$ is the DC component of the $\mathbf{G}$, and $M$ and $N$ are the number of rows and columns in $\mathbf{G}_0$. Now, the frequency domain representation of the zero mean RSS image can be obtained as $\mathbf{H}=DCT\{\mathbf{G}_0\}$, where $DCT\{\cdot\}$ defines the DCT operation as given in [21].

Since the dimensions of the frequency domain matrix $\mathbf{H}$ are known, we can also denote each matrix element by using a single index as $[\mathbf{H}]_j$ (e.g., in column-wise manner) instead of separate row and column indices. Furthermore, we collect all the matrix elements, which here are the DCT coefficients, into a DCT coefficient vector $\mathbf{h}$ as $[\mathbf{h}]_j=[\mathbf{H}]_j$ for $j=0,1,\ldots,M\cdot N-1$. Because of the spatial correlation of the RSS measurements, a majority of the energy in $\mathbf{h}$ is concentrated on a few DCT coefficients. Therefore, in order to select the most significant DCT coefficients from $\mathbf{h}$, we rearrange the DCT coefficients in a descending energy-wise order so that

$$|[\mathbf{Th}]_j|^2 \geq |[\mathbf{Th}]_{j+1}|^2 \quad \text{for } j = 0,\ldots,MN-1, \quad (15)$$

where $\mathbf{T}$ is a permutation matrix defined as

$$[\mathbf{T}]_{pq} = \begin{cases} 1, & \text{if } [\mathbf{h}]_p \text{ has the } q^{\text{th}} \text{ largest energy} \\ 0, & \text{otherwise} \end{cases} . \quad (16)$$

Now, to achieve a desired compression ratio, only $N_{coef}$ first elements of $\mathbf{Th}$, that is $[\mathbf{Th}]_0$, $[\mathbf{Th}]_1,\ldots,[\mathbf{Th}]_{N_{coef}-1}$, are stored in the database for the considered TX. The choice of the optimum number of DCT coefficients $N_{coef}$ is further studied in Section 4.

The computational effort of the proposed spectral compression approach is mainly on the DCT transformation and in sorting the DCT coefficients in an energy-wise order. Therefore, it is clear that the computational effort of the proposed method is relatively low compared to other compression methods, such as the clustering-based methods discussed in [15]-[16].

In the localization phase the original RSS image can be reconstructed from the stored DCT coefficients. First, we define the reconstructed frequency domain RSS image as

$$[\hat{\mathbf{H}}]_j = \begin{cases} [\mathbf{h}]_j & \text{if } 1 \in \{[\mathbf{T}]_{jq} : q = 0,\ldots,N_{coef}-1\} \\ 0, & \text{otherwise} \end{cases} , \quad (17)$$

where $[\hat{\mathbf{H}}]_j$ can be seen as a sparse matrix where only the stored DCT coefficients are included. Second, we take the inverse DCT to obtain the recovered zero mean RSS image as $\hat{\mathbf{G}}_0=IDCT\{\hat{\mathbf{H}}\}$ as given in [21]. Finally, we add the stored DC-component and get the compressed RSS image as $\hat{\mathbf{G}}=\hat{\mathbf{G}}_0+\mu$. Similar to the compression of the RSS image, the computational complexity of reconstructing the RSS image is very low, as the main effort is in computing the inverse DCT with relatively low matrix sizes.

To study how the spectral compression affects the variance of the location likelihood function, it is convenient to divide the zero mean RSS image into sub-components according to the measurement model given in (1) as

$$\mathbf{G}_0 = \mathbf{Q} + \mathbf{S} + \mathbf{W} = \mathbf{U} + \mathbf{W}, \quad (18)$$

where $\mathbf{Q}$, $\mathbf{S}$, $\mathbf{W}$ and $\mathbf{U}$ are matrices of the same size with $\mathbf{G}_0$, describing the PL model term, the stationary shadowing term, time-variant shadowing term, and the localization relevant term of the zero mean RSS image, respectively. Here, $\mathbf{U}$ includes all the relevant information for the localization, since it remains unchanged from the learning phase to the localization phase. Whereas in the PL modelling approach only the PL model part is considered to be stored in the learning database, in the spectral compression approach both the PL model $\mathbf{Q}$ and the stationary shadowing $\mathbf{S}$ are captured jointly. However, due

to lossy data compression, the stored DCT coefficients are able to present only a certain portion of the information included in **Q** and **S**.

Due to the linearity of the DCT operation, we can calculate the DCT separately for each term in (18) and write

$$\mathbf{H} = DCT\{\mathbf{G}_0\} = DCT\{\mathbf{U}\} + DCT\{\mathbf{W}\} = \mathbf{H}_\mathbf{U} + \mathbf{H}_\mathbf{W}, \quad (19)$$

where $\mathbf{H}_\mathbf{U}$ and $\mathbf{H}_\mathbf{W}$ are the frequency domain images for the **U** and **W**. Moreover, by considering separately the compressed image and its residual matrix after the compression, we are able to write

$$\mathbf{H} = \hat{\mathbf{H}} + \tilde{\mathbf{H}} = \hat{\mathbf{H}}_\mathbf{U} + \hat{\mathbf{H}}_\mathbf{W} + \tilde{\mathbf{H}}_\mathbf{U} + \tilde{\mathbf{H}}_\mathbf{W}, \quad (20)$$

where $\tilde{\mathbf{H}}$ is the frequency domain residual matrix defined as

$$[\tilde{\mathbf{H}}]_j = \begin{cases} [\mathbf{h}]_j & \text{if } 1 \notin \{[\mathbf{T}]_{jq} : q = 0,\ldots,N_{coef}-1\} \\ 0, & \text{otherwise} \end{cases}, \quad (21)$$

which consists of those DCT coefficients which are not stored in the database. Additionally, $\hat{\mathbf{H}}_\mathbf{U}$ and $\hat{\mathbf{H}}_\mathbf{W}$ are the useful part and the noise part of the compressed image $\hat{\mathbf{H}}$, and $\tilde{\mathbf{H}}_\mathbf{U}$ and $\tilde{\mathbf{H}}_\mathbf{W}$ are the compression error part and the noise part of the residual image $\tilde{\mathbf{H}}$. Thus, the more DCT coefficients are stored in the database the more energy of the useful part is preserved. However, with each new stored DCT coefficient also the noise level of the database is increased as the number of non-zero elements in $\hat{\mathbf{H}}_\mathbf{W}$ increases. Conversely, any zero elements in $\hat{\mathbf{H}}_\mathbf{W}$ (i.e., discarded DCT coefficients in the compression) reduce the amount of overall noise in the learning database. This type of a noise filtering, together with appropriate DCT coefficient selection, is able to improve the localization performance compared to the conventional fingerprinting, even though the overall size of the database is reduced.

In the spectral compression approach, the variance of the probability density function $p_{RSS,r,i}(\cdot)$ in the likelihood function, given in (8) depends on the realized compression error and the variance of the filtered noise. Based on (1), the learning data RSS values at each location are Gaussian distributed, and thus, also the compression error is Gaussian distributed. This is, because the DCT is a linear operator, which means that also the elements of the frequency domain image **H**, and consequently the elements of the compression error matrix $\tilde{\mathbf{H}}_\mathbf{U}$, are Gaussian distributed. Thus, for the spectral compression approach, the variance of the $p_{RSS,r,i}(\cdot)$ is given as

$$\sigma_{IM}^2 = \sigma_{cErr}^2 + \sigma_{wFil}^2 + \sigma_W^2, \quad (22)$$

where $\sigma_{cErr}^2$ is the variance of the compression error and $\sigma_{wFil}^2$ ($\leq \sigma_W^2$) is the variance of the filtered noise. Here, due to the fact that the noise term $W$ is white, the noise spectrum is flat and the noise filtering affects equally to all coordinates. With appropriate DCT coefficient selection, similar whiteness can also be approximated for the compression error. However, more detailed analysis of the compression error and noise filtering are conducted in Section 4.

As shown in [21], the localization with the spectrally compressed RSS images can be performed by using the reconstructed RSS images to recover the learning data for each location and TX. Therefore, the location estimate can be attained from (11), similar to the fingerprinting and the PL modeling approaches.

### 3.3 Database sizes for the considered localization approaches

#### 3.3.1 Fingerprinting

Since each fingerprint consists of location coordinates (i.e. x and y coordinates) and the indices of the heard TXs with their corresponding RSS values, the size of the required fingerprint database in terms of stored real valued numbers can be defined as

$$B_{FP} = \sum_{i=0}^{N_{FP}-1} (2+2N_{TX,i}), \quad (23)$$

where $N_{TX,i}$ is the number of heard TXs in the $i^{\text{th}}$ fingerprint.

#### 3.3.2 PL-model-based approach

Compared to the fingerprinting approach the required size of the learning database can be greatly reduced by exploiting the PL models. In this case only the TX location coordinates and the PL parameters $A$ and $n$ have to be stored for each heard TX. Therefore, the number of stored real valued numbers for the PL modeling approach can be calculated as

$$B_{PL} = 4N_{TX}. \quad (24)$$

#### 3.3.3 Spectrally compressed RSS images

The size of the required learning database for the spectrally compressed RSS images depends on how many DCT coefficients are stored per each TX. However, as defined in [21], the number of real valued numbers stored in the learning database can be defined as

$$B_{IM} = \sum_{r=0}^{N_{TX}-1} 6+2N_{coef,r} \quad (25)$$

where $N_{coef,r}$ is the number of stored DCT coefficients for the $r^{\text{th}}$ TX. This is, because each RSS image requires information on the TX identity, the image location, image dimensions, image mean, and the stored DCT coefficient values and their indices. If there is a large number of RSS values per each TX found in the learning database, the spectral compression approach is able to approximate the same information with only a few number of DCT coefficients.

## 4 Selection of the DCT Coefficients

### 4.1 Compression error distribution and noise distribution

Based on (19), the residual matrix of the RSS image $\mathbf{G}_0$, discarded in the compression process, can be obtained by the inverse DCT as

$$\tilde{\mathbf{G}} = IDCT\{\tilde{\mathbf{H}}\} = IDCT\{\tilde{\mathbf{H}}_\mathbf{U}\} + IDCT\{\tilde{\mathbf{H}}_\mathbf{W}\}. \quad (26)$$

Here, the energy of the noise term $IDCT\{\tilde{\mathbf{H}}_\mathbf{W}\}$ is uniformly distributed in the whole image area, since $W$ has been considered as white Gaussian noise. If the number of stored DCT coefficients is sufficient, and thus, most of the energy of **U** is preserved, the compression error $IDCT\{\tilde{\mathbf{H}}_\mathbf{U}\}$ can also be approximated as white Gaussian noise. As an example, in Fig. 2 we have plotted the autocorrelation function of the

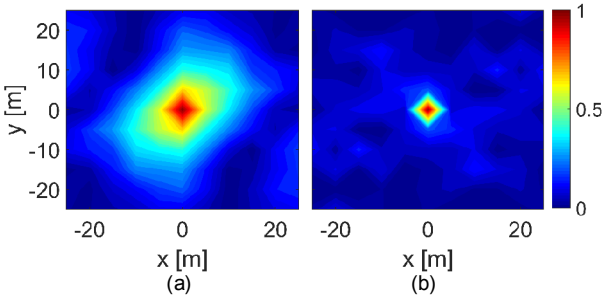


Fig. 2. An example of the autocorrelation function of the residual RSS image error $\tilde{\mathbf{G}}$ for (a) $N_{coef}$=2 and (b) $N_{coef}$=20.

residual matrix $\tilde{\mathbf{G}}$ for one TX in the experimental measurement set with two different numbers of stored coefficients. Now, when the number of stored coefficients is adequate ($N_{coef}$=20), the autocorrelation function appears as a narrow impulse (indicating whiteness), but when only a few coefficients ($N_{coef}$=2) are stored, the autocorrelation function is considerably wider and it reflects the spatial correlation function of the radio propagation channel. Moreover, in the latter case, based on (20), the error residual $\tilde{\mathbf{G}}$ resembles the original RSS image, since most of the DCT coefficients are included in the residual term $\tilde{\mathbf{H}}$, instead of the compressed image term $\hat{\mathbf{H}}$. Here, it is worth of noticing that using the assumption of whiteness for the noise term $W$, it is possible to find an appropriate estimate of the number of stored DCT coefficients $N_{\text{coef}}$ by studying the autocorrelation function. Since only the useful term $\mathbf{U}$ is spatially correlated, $N_{\text{coef}}$ can be iteratively increased until the autocorrelation function appears close to an impulse function. After this, all extra DCT coefficients can be expected to consist of mostly noise.

### 4.2 Cumulative energy of the sorted DCT coefficients

The question of how many DCT coefficients should be stored per each RSS image is fundamentally a trade-off between the desired compression ratio and SNR (i.e., the ratio between the useful information $\mathbf{U}$ and the noise term $\mathbf{W}$) of the database. To study this trade-off in more detail, we consider the energy-wise sorted DCT coefficient vector $\mathbf{Th}$ defined earlier in (15). In Fig. 3 we have illustrated the cumulative energy of the sorted DCT coefficients, given as

$$E_{TOT,k} = \frac{\sum_{j=0}^{k-1} \left|[\mathbf{Th}]_j\right|^2}{\sum_{j=0}^{MN-1} \left|[\mathbf{Th}]_j\right|^2}, \quad k = 1,2,...,MN \tag{27}$$

for the same TX in the experimental learning dataset, used earlier in Fig. 2, and where $E_{TOT,k}$ gives the cumulative energy of the first $k$ coefficients in percent of the total energy. It can be seen that a majority of the energy is concentrated in a small number of largest magnitude coefficients. However, studying the cumulative energy does not reveal the SNR of the DCT coefficients, and thus, does not unambiguously indicate how many coefficients should be stored in the learning database.

With the spectrally compressed RSS images we attempt to compress and store only the useful part $\mathbf{U}$. Hence, it would be ideal to sort the DCT coefficients based on $\mathbf{H}_{\text{U}}$ only, but due to the presence of the additive noise term $\mathbf{H}_{\text{W}}$, this is not possible. Moreover, because majority of the energy of $\mathbf{H}_{\text{U}}$ is concentrated on a small number of DCT coefficients, it is evident that at some point in the cumulative energy curve, the noise term $\mathbf{H}_{\text{W}}$ begins to dominate the sorting process.

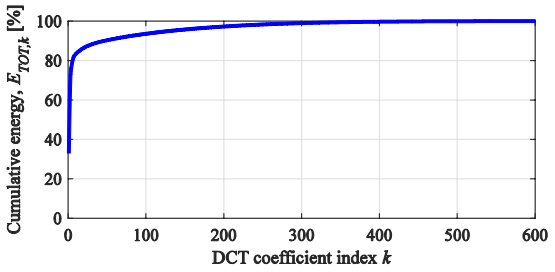


Fig. 3. An example of the cumulative Energy of the sorted DCT coefficients.

### 4.3 Distribution of energy between the useful part and the noise part of the DCT coefficients

In practice, the analysis of the distributions of the useful information $\mathbf{U}$ and the noise term $\mathbf{W}$ turns out to be extremely complicated. This is because the permutation matrix $\mathbf{T}$ depends on the arithmetic sum of the $\mathbf{U}$ and $\mathbf{W}$, which cannot be perfectly distinguished from each other in case of experimental RSS measurements. Therefore, to study how the useful information $\mathbf{U}$ and the noise $\mathbf{W}$ are shown in each DCT coefficient $[\mathbf{h}]_j$, we choose to use simulated RSS images. For this we exploit the methods studied in [35], where the RSS values are simulated by using an appropriate PL model and spatially correlated shadowing. In the following analysis we have considered the indoor case, where the TX location is chosen randomly and the PL model $\mathbf{Q}$ is defined according to (2) with $A$=-20dBm and $n$=3.5. In addition, we have added correlated shadowing $\mathbf{S}$ by using the correlation model given in (4) with $D_{corr}$=8m, and time-dependent shadowing $\mathbf{W}$ with $\sigma_W^2$ =4dB. Here we have assumed the database grid interval as $g_{INT}$=5m, and that only one RSS measurement is used per each grid point and $N_{MEAS,r,i} = 1, \forall i,r$. In Fig. 4 an outcome of the simulated RSS image $\mathbf{G}$ is illustrated. In addition, as an example, the figure also includes the DCT image and the reconstructed RSS image with 25 stored DCT coefficients.

First, in order to study how the useful information and the noise are distributed in the DCT coefficients, we divide the coefficient vector $\mathbf{h}$ of the zero mean RSS image $\mathbf{G}_0$ into the useful information term and the noise term, similar to (19), as

$$\mathbf{h} = \mathbf{h}_{\text{U}} + \mathbf{h}_{\text{W}}, \tag{28}$$

where $\mathbf{h}_{\text{U}}$ and $\mathbf{h}_{\text{W}}$ are the vectors containing the useful part and the noise part of the DCT coefficients.

At this point, it is worth of emphasizing that the sorting process along with the permutation matrix $\mathbf{T}$, are defined based on the total energy of $\mathbf{h}$, and consequently, the elements of $\mathbf{h}_{\text{U}}$ and $\mathbf{h}_{\text{W}}$ are not generally in energy-wise order. As an example, in Fig. 5 we have separately plotted the energy of each DCT coefficient for the useful part

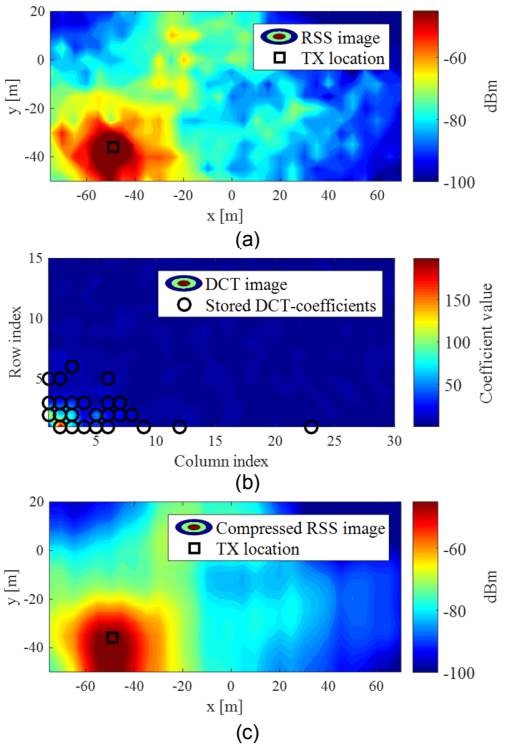


Fig. 4. An example of a simulated RSS image (a), Frequency-transformed image by using the DCT (b), and reconstructed RSS image by using 25 stored DCT coefficients (c).

$|[\mathbf{Th}_U]_j|^2$, the noise part $|[\mathbf{Th}_W]_j|^2$, and for the total energy $|[\mathbf{Th}]_j|^2$, for $j$=0,…,$M$·$N$-1. It can be seen that whereas the total energy is monotonically decreasing, the useful part and the noise part are not sorted in energy-wise order. In fact, due to the spatial correlation, the first 20-30 largest coefficients of the useful part $|[\mathbf{Th}_U]_j|^2$ are considerably larger than any the noise coefficients $|[\mathbf{Th}_W]_j|^2$. However, since the energy of the useful part is concentrated on these few first coefficients, after these the noise becomes the dominant component very quickly. The included noise threshold value is explained and discussed later in Section 4.5.

### 4.4 Energy of the compression error, the noise error and the total error

By considering (15), (16) and (28), and assuming that $N_{coef}$ largest magnitude DCT coefficients are stored in the database, we can write the overall energy of the compression error and the overall energy of the noise error respectively as

$$\varepsilon_{cErr,N_{coef}} = \|\mathbf{h}_U\|^2 - \sum_{j=0}^{N_{coef}-1} \left|[\mathbf{Th}_U]_j\right|^2 \quad , \qquad \varepsilon_{wFil,N_{coef}} = \sum_{j=0}^{N_{coef}-1} \left|[\mathbf{Th}_W]_j\right|^2 \tag{29}$$

where $\varepsilon_{cErr,N_{coef}}$ defines the overall energy of the compression error (i.e., the total energy of the discarded DCT coefficients), and $\varepsilon_{wFil,N_{coef}}$ defines the overall energy of the filtered noise error, when $N_{coef}$ largest elements are preserved. Moreover, the total error due to the compression error and the noise error can be simply given as

$$\varepsilon_{TOT,N_{coef}} = \varepsilon_{cErr,N_{coef}} + \varepsilon_{wFil,N_{coef}} \, . \tag{30}$$

In Fig. 6, we have presented separately the compression error, the noise error, and the total error for the previously considered simulated RSS image as a function of the number of stored DCT coefficients $N_{coef}$. From here it is clear that with a particular value of $N_{coef}$=30, and roughly with ±10 coefficients around it, the total error is roughly minimized. At this point, the steepest descend of the compression error has been achieved and the rate of the degradation of the compression error appears to level off gradually. Around at the same point, the noise error has an abrupt rise, since the noise becomes the dominating component of the DCT coefficient sorting process, and therefore, the largest noise components are typically found around this region. In addition, we have also included the total error energy of the fingerprinting approach in Fig. 6. With fingerprinting there is no compression error, but all the noise energy is present in the corresponding RSS values (i.e., the sum of all elements in $\mathbf{h}_W$). Nevertheless, it is clearly visible that the RSS image approach results in smaller overall error throughout the different values of $N_{coef}$ as long as the few largest DCT coefficients are stored in the database. Additionally, assuming that the noise variance $\sigma_W^2$ would be known, it would be possible to set the value of $N_{coef}$ based on the threshold defined by fingerprinting error energy. By this way the size of the database could be minimized while maintaining the condition that the localization accuracy is not degraded compared to the

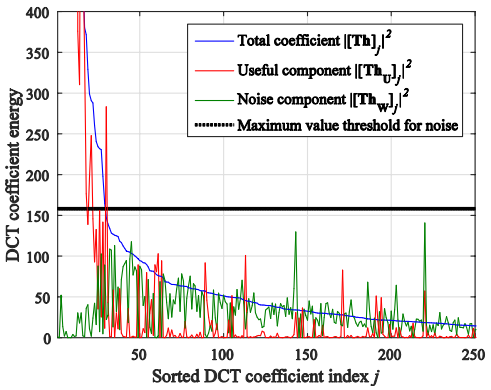


Fig. 5. Energy of the sorted DCT coefficients given separately for the useful part and the noise part. The definition of the maximum value threshold for the noise is considered later in Section 4.5.

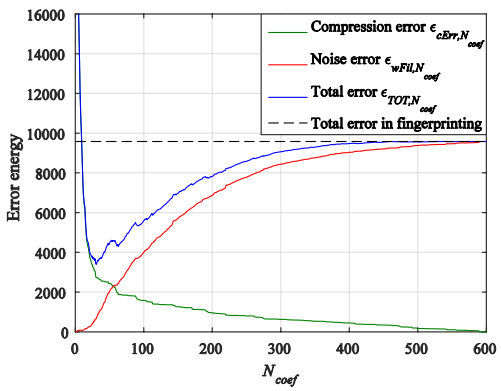


Fig. 6. The compression error, the noise error, and the total error of the compressed RSS image as function of the number of DCT coefficients $N_{coef}$.

fingerprinting. However, if the noise variance $\sigma_W^2$ is unknown, it can be estimated from the RSS data by using the assumption of whiteness of $W$. The number of stored DCT coefficients $N_{coef}$ can be also selected, for example, based on the number of original RSS measurements in the RSS image, as done in [21].

### 4.5 New probabilistic approach on selection of the optimum number of DCT coefficients

In practice we cannot separate between the useful part $\mathbf{h}_U$ and the noise part $\mathbf{h}_W$, but we are only able to observe the total cumulative energy of the DCT coefficients $E_{TOT,k}$, given in (27). Despite of this, we desire to find the optimum number of the stored DCT coefficients, which would minimize the total error, and thus, maximize the SNR of the learning database. Of course, depending on the desired compression ratio, it might also be preferred to select fewer coefficients than indicated by the minimum error point.

If we again study Fig. 5, it is obvious that when most of the energy in the useful information part $\mathbf{h}_U$ is preserved, the largest components in the noise part $\mathbf{h}_W$ begin to dominate the sorting process. Consequently, in case that the energy of the largest existing noise component could be estimated, it would be possible to approximate the index $j$ of the sorted DCT coefficients $[\mathbf{Th}]_j$, where the noise begins to dominate. To do this, we must study the statistical properties of the noise part $\mathbf{h}_W$ in more detail. In the following analysis we assume the knowledge of the variance of the noise term $\sigma_W^2$, which can be in practice estimated from the RSS measurements during the learning data collection phase by studying the RSS measurement sets $\Omega_{RSS,i,r}$ for each fingerprint and TX.

Since each noise component $[\mathbf{h}_W]_j$ is Gaussian distributed, the energy $|[\mathbf{h}_W]_j|^2$ is chi-squared distributed. Now, the estimate of the largest noise component $h_{W\max}=\max(\{|[\mathbf{h}_W]_j|^2 : j=0,\ldots,M\cdot N-1\})$ can be obtained as

$$\hat{h}_{W\max} = \sigma_W^2 F_\chi^{-1}(1-\lambda) \tag{31}$$

where $F_\chi^{-1}(\cdot)$ is the inverse chi-square cumulative density function and the probability $0<\lambda\leq 1$ is a specific design parameter used to adjust the level of $\hat{h}_{W\max}$. Moreover, $\lambda$ determines the probability of each element $|[\mathbf{h}_W]_j|^2$ being larger than $\hat{h}_{W\max}$. For example, if we choose $\lambda=0.01$, there is 1% chance that an arbitrarily taken $|[\mathbf{h}_W]_j|^2$ is larger than $\hat{h}_{W\max}$. Thus, by choosing $\lambda=1/(M\cdot N)$, where $M\cdot N$ is the number of the elements in $\mathbf{h}_W$, it is expected that exactly one element of $\mathbf{h}_W$ is larger than $\hat{h}_{W\max}$. This means that the number of stored DCT coefficients can be determined by using the noise energy threshold $\hat{h}_{W\max}$ and the energy of the sorted DCT coefficients $|[\mathbf{Th}]_j|^2, j=0,\ldots,M\cdot N-1$ so that

$$\hat{N}_{coef} = \arg\min_j \left( \left| [\mathbf{Th}]_j \right|^2 - \hat{h}_{W\max} \right), \tag{32}$$

where $\hat{N}_{coef}$ is the estimated number of stored DCT coefficients in the database. Basically, here we choose the first $\hat{N}_{coef}$ elements from the sorted DCT coefficient vector up until the coefficient energy falls under the threshold $\hat{h}_{W\max}$. In Fig. 5, this threshold was earlier illustrated for the simulated RSS image. It can be clearly seen that the noise components become dominating after the DCT coefficient energy crosses the threshold. In this specific case the achieved value for the number of stored coefficients is obtained as $\hat{N}_{coef}=29$, which is around the point of the minimum total error, shown in Fig 5. Therefore, the proposed probabilistic DCT coefficient selection approach is also maximizing the SNR of the learning database.

## 5 Cramér-Rao Lower Bound for the Considered Localization Approaches

### 5.1 Derivation of Cramér-Rao Lower Bound

With CRLB we can find a lower bound for the variance of an unbiased location estimator [29]. For this we exploit the system model given in (1) and the likelihood function given in (8). Assuming that the variance of $p_{RSS,r,i}(\cdot)$ in the likelihood function does not alter between locations and between the TXs measured by the user, the Fisher information matrix $\mathbf{I}(x,y)$ of size 2×2 can be defined as

$$[\mathbf{I}(x,y)]_{ij} = \frac{1}{\sigma_{RSS}^2} \sum_{r\in\Omega_{TXheard}} \begin{bmatrix} \frac{\partial^2 U_r(x,y)}{\partial x^2} & \frac{\partial^2 U_r(x,y)}{\partial x \partial y} \\ \frac{\partial^2 U_r(x,y)}{\partial y \partial x} & \frac{\partial^2 U_r(x,y)}{\partial y^2} \end{bmatrix}, \tag{33}$$

where $\sigma_{RSS}^2$ is the variance of $p_{RSS,r,i}(\cdot)$, which varies between the considered localization approaches as given in (12), (13) and (22). Furthermore, $U_r(x,y)$ is the useful part of the RSS image, defined as $U_r(x,y)=Q_r(x,y)+S_r(x,y)$, where $Q_r(x,y)$ and $S_r(x,y)$ are defined as in (1), but for the $r^{\text{th}}$ observed TX. Here it should be noticed that $U_r(x,y)$, is unique for each set of heard TXs and for each radio propagation environment. Because of this, similar to the studies in Section 4.3, we use simulated RSS images to obtain $U_r(x,y)$ for each heard TX. Moreover, due to the uniqueness of $U_r(x,y)$ in different radio environments, also the CRLB varies along with the environment and no general bound for the localization accuracy can be found.

Since the simulated RSS images consist of samples from the target area, we can approximate $U_r(x,y)$ as a piecewise-defined 3D surface with x-coordinates, y-coordinates and $U_r(x,y)$. This can be considered to be equivalent with the Delaunay-triangulation-based 2D interpolation, where the triangular faces compose the piecewise-defined 3D surface. Therefore, for the $m^{\text{th}}$ triangle of the triangulation (i.e., the area between 3 nearby coordinates), we approximate the $U_r(x,y)$ by a plane function as

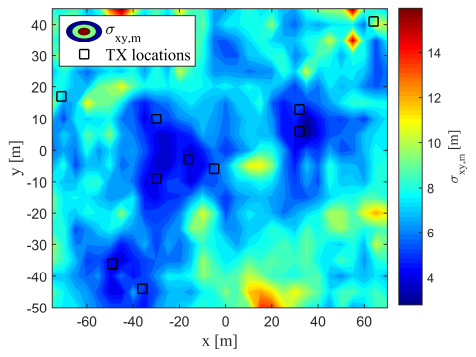


Fig. 7. An example realization of CRLB for 10 observed TXs in arbitrary locations.

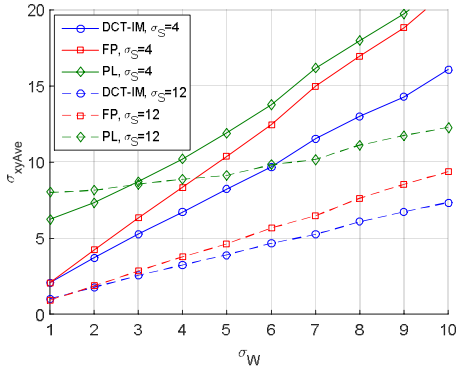


Fig. 8. CRLB as a function of the standard deviation of noise for different slow fading variances.

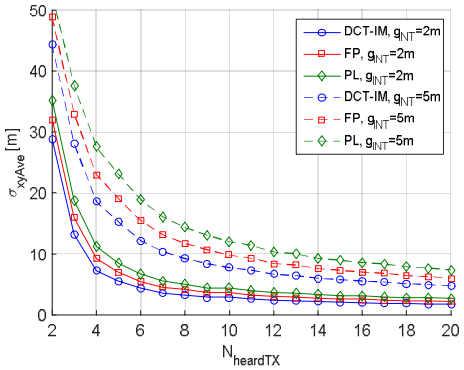


Fig. 9. CRLB as a function of heard TXs for different grid intervals.

$$U_r^{(m)}(x,y) = -\frac{a_r x + b_r y + d_r}{c_r}, \quad (34)$$

where $U_r^{(m)}(x,y)$ is the plane approximation for the $m^{\text{th}}$ triangle of the $r^{\text{th}}$ heard TX, and the coefficients $a_r$, $b_r$, $c_r$ and $d_r$ are determined so that the plane intersects the 3 points defined by the triangulation. Now, by using the plane approximation for the Fisher matrix definition in (33), the Fisher matrix for the $m^{\text{th}}$ piece-wise defined triangle area can be given as

$$[\mathbf{I}_m(x,y)]_{ij} = \frac{1}{\sigma_{RSS}^2} \sum_{r \in \Omega_{TXheard}} \frac{1}{c_r} \begin{bmatrix} a_r^2 & a_r b_r \\ a_r b_r & b_r^2 \end{bmatrix}. \quad (35)$$

From here the CRLB for the estimated x-coordinate and the y-coordinate can be obtained by taking the diagonal elements of the inverse of the Fisher matrix as

$$\sigma_{x,m}^2 \geq [\mathbf{I}_m^{-1}(x,y)]_{11} \text{ and } \sigma_{y,m}^2 \geq [\mathbf{I}_m^{-1}(x,y)]_{22}. \quad (36)$$

Similar to the studies in [25], for the 2D coordinate error we define the total location error variance as $\sigma_{xy,m}^2 = \sigma_{x,m}^2 + \sigma_{y,m}^2$.

In Fig. 7, we show an example of the CRLB $\sigma_{xy,m}$ for a single set of RSS measurements observed from 10 separate TXs in arbitrary locations. Here we have assumed the same radio environment parameters as with the simulated RSS images in sub-section 4.3. Moreover, we use the probabilistic DCT coefficient selection proposed in sub-section 4.5. It can be seen that the localization accuracy appears to be the highest close to the TX locations and generally 3m<$\sigma_{xy,m}$<16m. Thus, the localization accuracy is highly dependent on the true location of the user. For this reason we study the average CRLB defined over the whole simulated area as $\sigma_{xyAve}^2 = 1/(N \cdot M) \cdot \sum_m \sigma_{xy,m}^2$. Moreover, due to the dependency of the CRLB on each realization, we generate 1000 independent RSS image realizations from which the resulted $\sigma_{xyAve}^2$ is taken as the arithmetic mean.

In Fig. 8 we show the theoretical CRLB $\sigma_{xyAve}$ for the three considered localization approach (the DCT-compressed RSS images (DCT-IM), the fingerprinting (FP), and the PL modelling (PL)) as a function the noise standard deviation $\sigma_W$. We have included results with two different values of the stationary shadowing standard deviation: $\sigma_S = 4$dB and $\sigma_S = 12$dB. It can be seen that as the noise variance increases, the DCT-IM approach improves compared to the other approaches. This is because of the noise filtering property of the DCT-IM, which is emphasized with large noise variances. It is also clear that when the variance of the stationary shadowing is increased, the localization accuracy is generally improved. This is quite expected, since $S(x,y)$ creates RSS variations on top of the PL model, which is fixed between the learning phase and the localization phase. Thus, with higher variance the $S(x,y)$ emphasizes the RSS differences between nearby locations, and thus, it becomes easier to separate locations from each other based on the observed RSS values. Regarding our own experimental RSS measurements, we estimated the standard deviation of $S(x,y)$ and the noise $W$ to vary between $\sigma_S$=5-6dB and $\sigma_W$=3-5dB, respectively.

In Fig. 9 we present the same CRLB results as in Fig. 8, but now as a function of number of heard TXs $\Omega_{TXheard}$, and for two separate grid intervals: $g_{INT}$=2m and $g_{INT}$ =5m. Based on the results, as $\Omega_{TXheard}$ increases, the localization accuracy improves, but with large values of $\Omega_{TXheard}$ the improvement rate levels off. Also the effect of grid interval is evident and it corresponds with the intuition that the localization accuracy is improved as the grid interval is reduced. Of course, in practice there is a limit for improving the localization accuracy by only reducing the grid interval.

## 6 Results with the Experimental Measurement Set for the Considered Localization Approaches

To test the validity of the CRLB results, and consequently, to justify the considered RSS measurement model and the related analytical studies, we have also performed localization with the experimental RSS measurements described earlier in sub-section 2.1. To obtain complete RSS images from the scattered fingerprints (required for the DCT computation in the DCT-IM approach), we use the linear interpolation with minimum value extrapolation, described in [34]. Furthermore, in the DCT-IM we use the probabilistic DCT coefficient selection approach described in sub-section 4.5, since this was also used in defining the results for the CRLB. Because we have considered floor-wise RSS models throughout the paper, we assume that the user floor is always perfectly known.

If Fig. 10 we present the average localization error of the DCT-IM approach, as well as other database compression approaches, as a function of database compression ratio

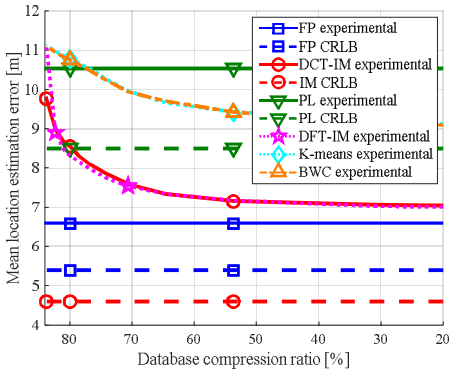


Fig. 10. Mean localization error averaged over all buildings as a function of the database compression ratio for the FP, DCT-IM, PL, DFT-IM, and clustering-based K-means BWC approaches. In addition, the CRLB levels $\sigma_{xyAve}$ for the FP, DCT-IM and PL approaches are approximated for the considered scenario.

with respect to the size of the fingerprinting database (i.e. 1-($B_{IM}$/$B_{FP}$) for the DCT-IM). The DCT-IM has been compared with the DFT-based approach (DFT-IM), and two clustering-based methods namely the K-means algorithm and the Block-based Weighted Clustering (BWC) algorithm [15]. Besides these, the average localization accuracies of the FP and PL methods have been provided as a baseline.

Here, the average error is determined as the average location error over all the buildings. The database compression ratio of the PL approach can be defined as high as 1-($B_{PL}$/$B_{FP}$)=95.5%, but the localization accuracy is clearly at far lower level compared to the other localization approaches. Because the used clustering approaches (i.e. K-means and BWC) require initialization of the cluster heads and optimization of specific design parameters, we have conducted a brief optimization procedure for the clustering algorithms in order to achieve the best possible results.

Different compression ratios with the DCT-IM and DFT-IM approaches are achieved by adjusting the value of the variance of the time-variant shadowing parameter $\sigma_W^2$ found in (31) in the probabilistic DCT coefficient selection process. The larger the assumed variance $\sigma_W^2$ is, the lower the number of stored DCT coefficients is to avoid the excessive rise in the noise energy. Similar variation of the compression ratio with the clustering algorithms is possible by selecting the number of used clusters. In the literature, the compression ratio for the clustering methods is often given with respect to the raw RSS measurements before the mapping into the grid points, whereas here we study the compression ratio with respect to the mapped grid points. Nevertheless, it is worth noticing that the computational complexity of the clustering approaches depend on the number of used clusters, and thus it varies according to the compression ratio. Moreover, the clustering-based approaches seem to have much larger computational complexity, as with the compression ratio of 50%, the clustering-based approaches took well over hundred times more computation time compared to the proposed DCT/DFT-based spectral compression approach.

In addition to the measurement-based results, we have also presented the CRLB $\sigma_{xyAve}$ for the considered localization approaches in Fig. 10 by assuming 10 heard TXs for each user measurement. These bounds are based on the average estimated standard deviations of $S(x,y)$ and $W$ as $\hat{\sigma}_S$=5.2dB and $\hat{\sigma}_W$=3.0dB, which were obtained from the measurement data. Here, it should be noticed that the average localization errors and the CRLBs in Fig. 10 are not directly comparable with each other, as the CRLB defines the minimum standard deviation (or variance) for the unbiased estimator (i.e. not the average localization error). Moreover, direct comparison between measurement-based localization results and the CRLB is generally extremely difficult, since each localization environment is unique. For example, besides the radio propagation parameters, the density and deployment of TXs affect the localization performance, as shown earlier in Fig. 7. In addition, whereas with the CRLB results we have assumed that the learning data is available everywhere in the target area, with the measurement-based results interpolation and extrapolation are used to complete the learning data.

The average localization errors of the DCT-IM and DFT-IM approaches are close to the errors in FP approach with compression rations of up to 70%. A higher compression ratio still works, but at the tradeoff of a poorer localization accuracy. A similar effect can also been seen with the clustering approaches, but the overall localization accuracy with the clustering approaches is at considerably lower level compared to the proposed spectral compression methods. Therefore, when taking into account the high computational complexity, requirement for parameter optimization, and relatively low localization accuracy, the spectral compression approach seems to provide a more attractable approach for a globally scalable indoor localization system. Since we have considered different

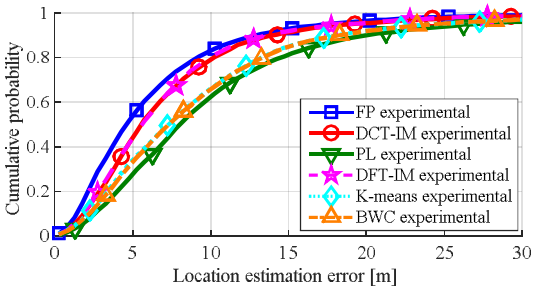


Fig. 11. Cumulative localization error over all buildings with compression ratio of 70% for the FP, DCT-IM, PL, DFT-IM, and clustering-based K-means and BWC approaches.

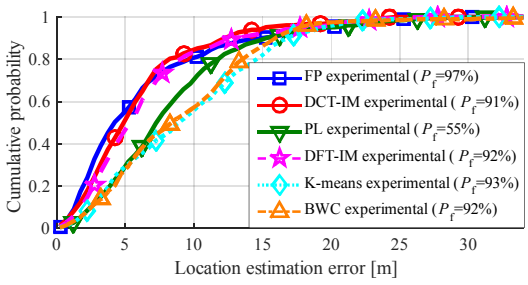


Fig. 12. Cumulative localization error and floor detection probability $P_f$ for the considered localization approaches in the 4-storey university building, in which multiple devices are used to collect the learning data and the user tracks. With database compression methods, the compression ratio is defined as 70 %.

types of buildings in the experimental measurement data, including offices and shopping malls, we assume that results can be generalized to various other indoor scenarios.

In addition to the mean localization error, the cumulative error curves for all the considered localization approaches by using a compression ratio of 70% (for DCT-IM, DFT-IM, K-means and BWC) are shown in Fig. 11. Similar to the average localization error, the FP approach along with the proposed spectral compression methods (DCT-IM and DFT-IM) are dominating the localization performance. Moreover, the shapes of the cumulative error curves are relatively similar between all the considered approaches, which indicates that there are no significant differences in the location error distributions and the advantage of our method comes from a large compression ratio and a fast computational time, suitable to large-scale mobile-centric localization approaches.

In order to consolidate the justification of the proposed algorithms, we have collected additional measurements from the 4-storey university building by using 3 separate measurement devices as described in Section 2.1. First, a learning database is constructed based on independently collected measurement sets with the 3 devices. After this, with each device, test user tracks are independently collected in order to study the localization performance. In Fig. 12, cumulative localization error curves are shown for each considered localization approach by using 70% compression ratio with the database compression methods. Here, we do not consider analytical results, and hence, also the floor detection is included and the resulted floor detection probabilities $P_f$ are given in the legend for each localization approach. The floor detection probability is defined as the probability of finding the vertical coordinate estimate to be the closest to the true user floor.

As expected, the proposed DCT-IM and DFT-IM approaches are also able to perform extremely well in the multiple device scenario. This is mainly because of the inbuilt noise filtering property, which is able to mitigate the effect of undesired RSS variations due to the use of multiple measurement devices. On the contrary, it seems that the clustering approaches are especially sensitive to the RSS variations due to use of multiple devices. Furthermore, whereas the floor detection probabilities are rather comparable with the DCT-IM, DFT-IM, BWC, and K-means approaches (all within $P_f$=91-93%), the FP-approach provides the best detection probability ($P_f$=97%), and the PL-approach the worst detection probability ($P_f$=55%). However, the smallest average localization error of 6.2m is achieved with the DCT-IM approach, whereas FP, PL and BWC approaches achieve average errors of 6.5m, 8.6m and 9.1m, respectively.

## 7 Conclusion

In this paper we have studied spectrally compressed RSS images, which can be exploited in several mobile-centric use cases from network-based localization to radio resource management in wireless networks. First, we introduced a measurement model for the observed RSS values. After this, we used the model for a detailed analysis of the spectral compression and derived the expressions for the compression error, noise error and total error in the compression process. In addition to this, we proposed a probabilistic method to select the optimum number of DCT coefficients to be stored in the database in order to maximize the database SNR.

Theoretical analysis was completed by deriving the CRLB for the considered localization approaches. To support the theoretical results, we also tested the proposed algorithms with the experimental RSS measurement set taken from 5 separate multi-storey buildings. Despite of the lossy compression, it was shown that with spectrally compressed RSS images it is possible to achieve a comparable localization error compared to the fingerprinting approach. This is due to the shown noise filtering property of the spectral compression, which affects the SNR of the learning database. Moreover, based on the experimental results including the effect of using multiple devices for collecting the data, the proposed compression algorithms provided comparable performance with the fingerprinting approach at a much lower complexity.

Although the spectral compression is already showing excellent performance by reducing the database size up until 70-80% with comparable performance with the FP approach, there is still potential for improvements. Firstly, before the DCT, it would be advantageous to take the physical radio environment into account when performing the interpolation and extrapolation of the RSS images. Secondly, by studying more sophisticated random value distributions instead of the Gaussian assumptions in the RSS measurement model, it could be possible to improve the accuracy of the measurement model.

## Acknowledgment

The authors express their warm thanks to the Academy of Finland (project 303576) for its financial support and to HERE for providing the measurement equipment.

## References

[1] S. Tang, H. Tan and L. Li, "A novel memory compression technique for embedded system," in *Proc. 2012 Second Int. Conf. Digital Inform. Commun. Technol. Applicat.*, 2012, pp. 287-292.

[2] M.A. Al-Ammar, S. Alhadhrami, A. Al-Salman, A. Alarifi, H.S. Al-Khalifa, A. Alnafessah and M. Alsaleh, "Comparative Survey of Indoor Positioning Technologies, Techniques, and Algorithms," in *Proc. 2014 Int. Conf. Cyberworlds*, 2014, pp. 245-252.

[3] Z. Farid, R. Nordin and M. Ismail, "Recent Advances in Wireless Indoor Localization Techniques and System," *J. Comput. Networks. Commun.*, vol. 2013, Article ID 185138, 2013.

[4] S. He and S.-H.G. Chan, "Wi-Fi Fingerprint-based Indoor Positioning: Recent Advances and Comparisons," *IEEE Commun. Surveys Tutorials*, vol. 18, no. 1, pp. 466-490, 2015.

[5] C. Liu et al., "RSS Distribution-Based Passive Localization and Its Application in Sensor Networks," *IEEE Trans. Wireless Commun.*, vol. 15, no. 4, pp. 2883-2895, Apr., 2016.

[6] S. Alletto et al., "An Indoor Location-Aware System for an IoT-Based Smart Museum," *IEEE Internet Things J.*, vol. 3, no. 2, pp. 244-253, Apr., 2016.

[7] H. Zou, B. Huang, X. Lu, H. Jiang and L. Xie, "A Robust Indoor Positioning System Based on the Procrustes Analysis and Weighted Extreme Learning Machine," *IEEE Trans. Wireless Commun.*, vol. 15, no. 2, pp. 1252-1266, Feb., 2016.

[8] K. Kaemarungsi and P. Krishnamurthy, "Modeling of indoor positioning systems based on location fingerprinting," IEEE Int. Conf. Comput. Commun., 2004, pp. 1012-1022.
[9] *Technical Specification Group Services and System Aspects;Evaluation of path-loss technologies for Location Services(LCS)(Release 9)*, 3GPP TR 25.907, 2010.
[10] H. Nurminen, J. Talvitie, S. Ali-Loytty, P. Muller, E. Lohan, R. Piche and M. Renfors, "Statistical path loss parameter estimation and positioning using RSS measurements in indoor wireless networks," in *Proc. 2012 Int. Conf. Indoor Positioning and Indoor Navigation*, 2012, pp. 1-9.
[11] S. Sun et al., "Investigation of Prediction Accuracy, Sensitivity, and Parameter Stability of Large-Scale Propagation Path Loss Models for 5G Wireless Communications," *IEEE Trans. Veh. Technol.*, vol. 65, no. 5, pp. 2843-2860, May, 2016.
[12] P. Bahl and V.N. Padmanabhan, "RADAR: an in-building RF-based user location and tracking system," in *Proc. Nineteenth Annu. Joint Conf. IEEE Computer and Commun. Societies INFOCOM 2000*, 2000, pp. 775-784 vol.2.
[13] K. Li, J. Bigham and L. Tokarchuk, "Validation of a Probabilistic Approach to Outdoor Localization," *IEEE Wireless Commun. Lett.*, vol. 2, no. 2, pp. 167-170, Apr., 2013.
[14] T. Roos, P. Myllymaki, H. Tirri, P. Misikangas and J. Sievanen, "A Probabilistic Approach to WLAN User Location Estimation," *Int. J. Wireless Inform. Networks*, vol. 9, no. 3, pp. 155-163, July, 2002.
[15] A. Arya, P. Godlewski, M. Campedel and G. du Chéné, "Radio Database Compression for Accurate Energy-Efficient Localization in Fingerprinting Systems," *IEEE Trans. Knowl. Data Eng.*, vol. 25, no. 6, pp. 1368-1379, June 2013.
[16] M. A. Youssef, A. Agrawala and A. Udaya Shankar, "WLAN location determination via clustering and probability distributions," in *Proc. First IEEE Int. Conf. Pervasive Computing Commun.*, 2003, pp. 143-150.
[17] Y. Zhang, Y. Zhu, M. Lu and A. Chen, "Using compressive sensing to reduce fingerprint collection for indoor localization," *2013 IEEE Wireless Commun. Networking Conf.*, 2013, pp. 4540-4545.
[18] C. Feng, W. S. A. Au, S. Valaee and Z. Tan, "Received Signal Strength based Indoor Positioning using Compressive Sensing," *IEEE Trans. Mobile Comput.*, vol. 11, no. 12, pp. 1983-1993, Dec., 2012.
[19] D. Milioris et al., "Low-dimensional Signal-Strength Fingerprint-based Positioning in Wireless LANs", *Elsevier Ad Hoc Networks*, Vol. 12, pp. 100-114, Jan., 2014.
[20] S. Nikitaki et al., "Efficient Multi-Channel Signal Strength based Localization via Matrix Completion and Bayesian Sparse Learning," *IEEE Trans. Mobile Comput.*, vol. 14, no. 11, pp. 2244-2256, Nov., 2015.
[21] J. Talvitie, M. Renfors and E. S. Lohan, "Novel Indoor Positioning Mechanism Via Spectral Compression," *IEEE Commun. Lett.*, Vol. 20, No. 2, pp. 352-355, Feb. 2016.
[22] *IEEE Standard for Information technology–Telecommunications and information exchange between systems Local and metropolitan area networks–Specific requirements Part 11: Wireless LAN Medium Access Control (MAC) and Physical Layer (PHY) Specifications*, IEEE Standard 802.11-2012, 2012.
[23] The Signal Processing for wireless positioning group, open-source software and measurement data. [Online]. Available: http://www.cs.tut.fi/tlt/pos/Software.htm. Accessed: Feb. 20, 2017.
[24] S. Jung, C. Lee and D. Han, "Wi-Fi fingerprint-based approaches following log-distance path loss model for indoor positioning," in *Proc. 2011 IEEE MTT-S Int. Microwave Workshop Series Intelligent Radio for Future Personal Terminals*, 2011, pp. 1-2.
[25] M. B. Zeytinci, V. Sari, F. K. Harmanci, E. Anarim and M. Akar, "Location estimation using RSS measurements with unknown path loss exponents," *EURASIP J. on Wireless Commun. and Networking*, 2013.
[26] M. Gudmundson, "Correlation model for shadow fading in mobile radio systems," *Electron. Lett.*, vol. 27, no. 23, pp. 2145-2146, Nov., 1991.
[27] J. Luo and X. Zhan, "Characterization of Smart Phone Received Signal Strength Indication for WLAN Indoor Positioning Accuracy Improvement," *J. Networks.*, vol. 9, no. 3, Mar., 2014.
[28] E. S. Lohan, J. Talvitie, P. Figueiredo e Silva, H. Nurminen, S. Ali-Loytty and R. Piche, "Received Signal Strength Models for WLAN and BLE-based Indoor Positioning in Multi-floor Buildings," in *Proc. Int. Conf. Localization and GNSS*, pp. 1-6, 2015.
[29] S.M. Kay, *Fundamentals of Statistical Signal Processing: Estimation Theory*, Upper Saddle River, NJ, USA: Prentice Hall, 1993.
[30] V. Honkavirta, T. Perala, S. Ali-Loytty and R. Piche, "A comparative survey of WLAN location fingerprinting methods," in *Proc. 6th Workshop Positioning, Navigation and Communication*, 2009, pp. 243-251.
[31] M.W. Bern, D. Eppstein, L.J. Guibas, J. Hershberger, S. Suri and J. Wolter, "The Centroid of Points with Approximate Weights," in *Proc. Third Annu. Eur. Symp. Algorithms*, 1995, pp. 460-472.
[32] C. Evrendilek and H. Akcan, "On the Complexity of Trilateration with Noisy Range Measurements," *IEEE Commun. Lett.*, vol. 15, no. 10, pp. 1097-1099, Oct., 2011.
[33] H. Staras and S.N. Honickman, "The accuracy of vehicle location by trilateration in a dense urban environment," *IEEE Trans. Veh. Technol.*, vol. 21, no. 1, pp. 38-43, Feb., 1972.
[34] J. Talvitie, M. Renfors and E.S. Lohan, "Distance-based Interpolation and Extrapolation Methods for RSS-Based Localization with Indoor Wireless Signals," *IEEE Trans. Veh. Technol.*, vol. 64, no. 4, pp. 1340-1353, Apr. 2015.
[35] J. Talvitie and E.S. Lohan "Modeling Received Signal Strength Measurements for Cellular Network based Positioning," in *Proc. Int. Conf. Localization and GNSS*, Turin, Italy, pp. 1-6, 2013.

**Jukka Talvitie** (S'08–M'16) received his M.Sc. degree in Automation engineering and Ph.D. in Computing and Electrical Engineering in Tampere University of Technology (TUT), Finland, in 2008 and 2016, respectively. He is currently a postdoctoral researcher at the Laboratory of Electronics and Communications Engineering at TUT, Finland. His main research interests include signal processing for communications, radio localization and 5G mobile cellular networks.

**Markku Renfors** (S'77–M'82–SM'90–F'08) received the Dr. Tech. degree from Tampere University of Technology (TUT), Finland, in 1982. Since 1992, he has been a Full Professor with the Laboratory of Electronics and Communications Engineering at TUT. His research interests include advanced waveforms for future wireless systems and signal processing algorithms for flexible communications transceivers and positioning devices.

**Mikko Valkama** (S'99–M'02–SM'15) received the M.Sc. and Ph.D. degrees (both with honors) in Electrical Engineering (EE) from Tampere University of Technology (TUT), Finland, in 2000 and 2001, respectively. Currently, he is a Full Professor and Laboratory Head at the Laboratory of Electronics and Communications Engineering at TUT, Finland. His general research interests include radio communications, communications signal processing, radio localization, and 5G mobile cellular radio networks.

**Elena Simona Lohan** (S'00, M'06, SM'13 ) received an M.Sc. degree in Electrical Engineering from Polytechnics University of Bucharest, Romania, in 1997, a D.E.A. degree (French equivalent of master) in Econometrics, at Ecole Polytechnique, Paris, France, in 1998, and a Ph.D. degree in Telecommunications from Tampere University of Technology (TUT), Finland, in 2003. Dr. Lohan is now an Associate Prof. at the Laboratory of Electronics and Communication Engineering (ELT) at TUT. Her current research interests include wireless location techniques, Location Based Services and privacy-aware positioning solutions.